

Asynchronous warming and $\delta^{18}\text{O}$ evolution of deep Atlantic water masses during the last deglaciation

Jiaxu Zhang^{a,b,1,2}, Zhengyu Liu^{a,b,c}, Esther C. Brady^d, Delia W. Oppo^e, Peter U. Clark^f, Alexandra Jahn^{g,h}, Shaun A. Marcottⁱ, and Keith Lindsay^d

^aCenter for Climatic Research, University of Wisconsin–Madison, Madison, WI 53706; ^bDepartment of Atmospheric and Oceanic Sciences, University of Wisconsin–Madison, Madison, WI 53706; ^cAtmospheric Science Program, Department of Geography, Ohio State University, Columbus, OH 43210; ^dClimate and Global Dynamics Division, National Center for Atmospheric Research, Boulder, CO 80307; ^eDepartment of Geology and Geophysics, Woods Hole Oceanographic Institution, Woods Hole, MA 02543; ^fCollege of Earth, Ocean, and Atmospheric Sciences, Oregon State University, Corvallis, OR 97331; ^gDepartment of Atmospheric and Oceanic Sciences, University of Colorado Boulder, CO 80309; ^hThe Institute of Arctic and Alpine Research, University of Colorado Boulder, CO 80309; and ⁱDepartment of Geoscience, University of Wisconsin–Madison, Madison, WI 53706

Edited by Edouard Bard, Centre Européen de Recherche et d'Enseignement des Géosciences de l'Environnement, Aix-en-Provence, France, and accepted by Editorial Board Member Donald E. Canfield August 31, 2017 (received for review March 21, 2017)

The large-scale reorganization of deep ocean circulation in the Atlantic involving changes in North Atlantic Deep Water (NADW) and Antarctic Bottom Water (AABW) played a critical role in regulating hemispheric and global climate during the last deglaciation. However, changes in the relative contributions of NADW and AABW and their properties are poorly constrained by marine records, including $\delta^{18}\text{O}$ of benthic foraminiferal calcite ($\delta^{18}\text{O}_c$). Here, we use an isotope-enabled ocean general circulation model with realistic geometry and forcing conditions to simulate the deglacial water mass and $\delta^{18}\text{O}$ evolution. Model results suggest that, in response to North Atlantic freshwater forcing during the early phase of the last deglaciation, NADW nearly collapses, while AABW mildly weakens. Rather than reflecting changes in NADW or AABW properties caused by freshwater input as suggested previously, the observed phasing difference of deep $\delta^{18}\text{O}_c$ likely reflects early warming of the deep northern North Atlantic by $\sim 1.4^\circ\text{C}$, while deep Southern Ocean temperature remains largely unchanged. We propose a thermodynamic mechanism to explain the early warming in the North Atlantic, featuring a strong middepth warming and enhanced downward heat flux via vertical mixing. Our results emphasize that the way that ocean circulation affects heat, a dynamic tracer, is considerably different from how it affects passive tracers, like $\delta^{18}\text{O}$, and call for caution when inferring water mass changes from $\delta^{18}\text{O}_c$ records while assuming uniform changes in deep temperatures.

Atlantic water masses | last deglaciation | oxygen isotopes | deep ocean warming

A number of marine records provide evidence for major reorganizations of ocean circulation during the last deglaciation, especially changes in formation and transport of North Atlantic Deep Water (NADW) and Antarctic Bottom Water (AABW) (1, 2). Such deep water mass changes were particularly pronounced during Heinrich Stadial 1 (HS1; 17.5–14.7 ka), when a significantly reduced Atlantic Meridional Overturning Circulation (AMOC) (3) led to a strong cooling in the Northern Hemisphere coupled with a warming in the Southern Hemisphere. However, the relative contributions of NADW and AABW to changes in deep circulation and its impact on tracer transport are poorly constrained during HS1, which limits our understanding of crucial ocean thermodynamic and dynamic processes that drive heat and freshwater transport as well as the carbon cycle and ultimately, affect global climate (4, 5).

In addition to nutrient proxies, such as $\delta^{13}\text{C}$ and Cd/Ca, and kinematic tracers, such as $^{231}\text{Pa}/^{230}\text{Th}$, high-resolution deep sea benthic foraminiferal calcite ($\delta^{18}\text{O}_c$) records have also been commonly used to infer water mass changes (6–10). $\delta^{18}\text{O}_c$ changes are well-understood to reflect the combined influence of variations in deep water temperature and the oxygen isotopic composition of the water ($\delta^{18}\text{O}_w$). One notable feature of these $\delta^{18}\text{O}_c$ records below 3,000 m is the decrease in $\delta^{18}\text{O}_c$ at the start

of HS1 in the northern North Atlantic (NA) relative to that in the Southern Ocean (SO) (8). The cause of this phasing difference and its implication for abyssal water masses remain unclear, however, because of the difficulty of separating the effects of water temperature and $\delta^{18}\text{O}_w$ on the $\delta^{18}\text{O}_c$ signal. Some studies suggest that this phasing reflects changes in the deep ocean circulation pattern, namely a northward expansion of southern-sourced ^{18}O -depleted deep water in response to a reduced AMOC (6, 7). In contrast, others conclude that this phasing reflects changes in the isotopic composition of source waters, with northern-sourced ^{18}O -depleted waters continuing to fill much of the intermediate and deep Atlantic with a moderately reduced AMOC (8–10). Assessing the potential contribution of temperature to the $\delta^{18}\text{O}_c$ records requires the development of high-resolution temperature reconstructions (e.g., Mg/Ca) to isolate the $\delta^{18}\text{O}_w$ signal, but this has proven to be difficult for intermediate and deep ocean water masses (11). Here, we provide an independent means to evaluate this issue by using an isotope-enabled ocean general circulation model that simulates changes in both water-mass temperature and $\delta^{18}\text{O}_w$ in response to changes in ocean circulation during the last deglaciation.

Significance

The reorganizations of deep Atlantic water masses are widely thought to regulate glacial–interglacial climate changes. However, the pattern of reorganizations and their impact on ocean tracer transport remain poorly constrained by marine proxies. Our modeling study, which simulates the coevolution of water masses and oxygen isotopes during the last deglaciation, suggests that deglacial meltwater input causes both northern- and southern-sourced deep water transports to decrease. This reorganization pattern leads to asynchronous warming between the deep North and South Atlantic, which might have caused the observed deglacial phasing difference in deep water oxygen isotope records between these ocean basins. We further propose a mechanism to explain the early warming in the northern North Atlantic.

Author contributions: J.Z. and Z.L. designed research; J.Z. performed research; E.C.B., A.J., and K.L. developed the isotope tracer modules of the ocean model; J.Z., D.W.O., P.U.C., and S.A.M. analyzed data; and J.Z., Z.L., and P.U.C. wrote the paper with input from all coauthors.

The authors declare no conflict of interest.

This article is a PNAS Direct Submission. E.B. is a guest editor invited by the Editorial Board.

Data deposition: The decadal-mean model data reported in this paper can be accessed at <http://pike.aos.wisc.edu:8080/#/download/iPOP2-TRACE>. The full dataset is available from the author upon request.

¹Present address: Computational Physics and Methods (CCS-2) and Center for Nonlinear Studies (CNLS), Los Alamos National Laboratory, Los Alamos, NM 87545.

²To whom correspondence should be addressed. Email: jiaxu@lanl.gov.

This article contains supporting information online at www.pnas.org/lookup/suppl/doi:10.1073/pnas.1704512114/-DCSupplemental.

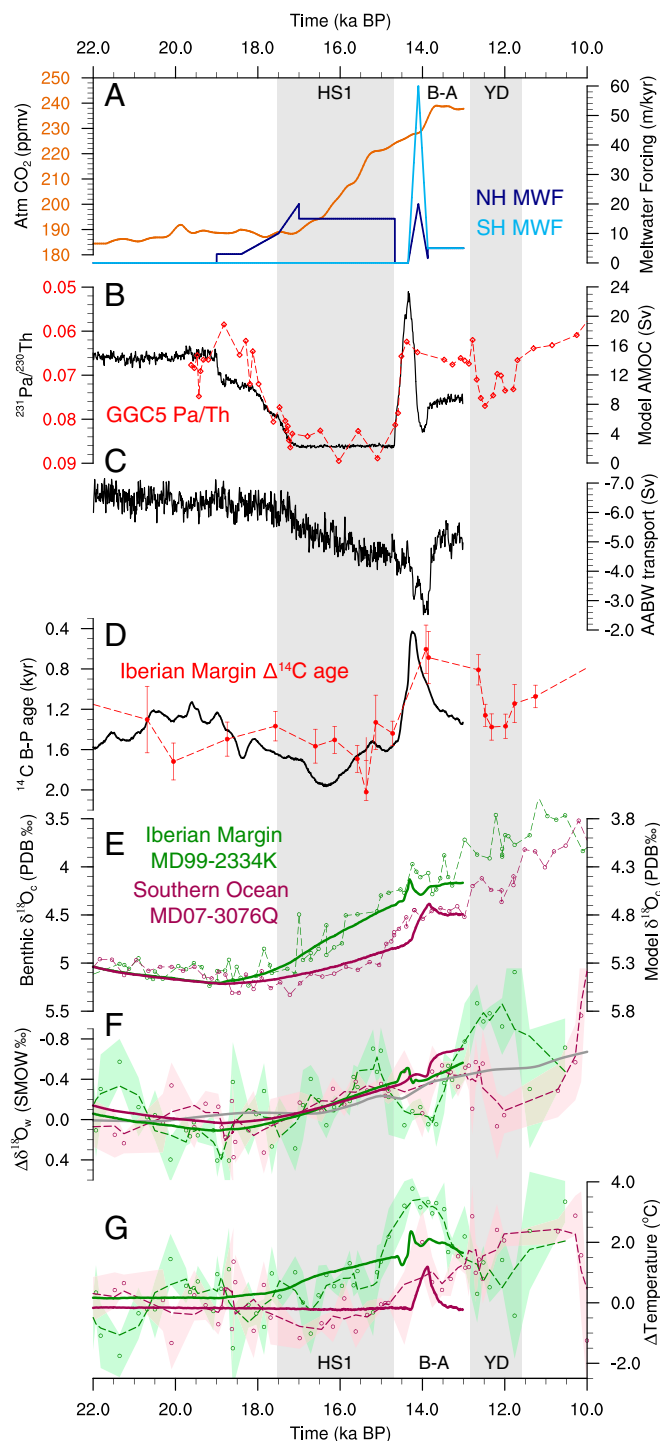


Fig. 1. Model deglacial signals compared with proxies. (A) Atmospheric CO₂ concentration (orange) and meltwater fluxes of the Northern (navy) Hemisphere (NH) and Southern (blue) Hemisphere (SH) (*SI Appendix, Table S1*) applied in TRACE21 (13). (B) Pa/Th ratio at Bermuda [GGC5 (3)] as a proxy for the strength of AMOC and model maximum AMOC transport (below 500 m). (C) Model AABW transport in the Atlantic basin (the minimum AMOC transport below 2,000 m). The negative values indicate counterclockwise circulation. (D) ¹⁴C benthic–planktonic (B–P) age offset at Iberian Margin [MD99-2334K (27)] and model abiotic ¹⁴C B–P age (44) at this site. (E) Benthic $\delta^{18}\text{O}_{\text{c}}$ at Iberian Margin [MD99-2334K (6, 31); green] and SO [MD07-3076Q (5, 8); pink] and the corresponding model $\delta^{18}\text{O}_{\text{c}}$. (F) Reconstructed deep water $\delta^{18}\text{O}_{\text{w}}$ anomalies (respective LGM mean was subtracted) at MD99-2334K (6) and MD07-3076Q (32) compared with the corresponding model $\delta^{18}\text{O}_{\text{w}}$ anomalies. Open circles represent the raw data, shaded areas represent the

Isotope-Enabled, Transient Ocean Simulation

Numerous modeling studies have explored possible forcing mechanisms involved in the deglacial evolution of the ocean (12–17). One challenge faced by these models is in comparing and validating their results directly against proxy records, either because the models do not simulate the same geotracers estimated by proxies or because those models that simulate proxy-related geotracers are forced by idealized climate forcing (e.g., idealized freshwater perturbations for a few 100 y). We address this challenge by enhancing a start-of-the-art ocean general circulation model (Parallel Ocean Program version 2) with the capability of simulating $\delta^{18}\text{O}_w$ and conducting a first 3D, isotope-enabled, transient ocean simulation with realistic geometry and forcing conditions.

We first implemented an oxygen isotope module in Parallel Ocean Program version 2 (iPOP2), where $\delta^{18}\text{O}_w$ is forced by the isotopic fluxes at the ocean surface and passively transported in the ocean interior, and then validated iPOP2 under present-day climate conditions. We next forced iPOP2 with $\delta^{18}\text{O}_w$ at 0‰ under Last Glacial Maximum (LGM; ~22 ka) climate conditions (iLGMspin), with $\delta^{18}\text{O}$ composition of hydrological variables (precipitation, evaporation, and river runoffs) constructed based on an isotope-enabled atmospheric model (18) under LGM conditions. We stopped iLGMspin after 4,000 y when $\delta^{18}\text{O}_w$ reached a global volume-mean value of 1.05‰, within the uncertainties of the reconstructed LGM value of $1.0 \pm 0.1\text{‰}$ (19), but before it reached full equilibrium.

Starting from the LGM state at 22 ka, we performed a transient simulation (iPOP2-TRACE) to the late Bølling–Allerød Interstadial at 13 ka under monthly varying surface boundary conditions, which were taken from a fully coupled climate simulation TRACE21. TRACE21 is a transient simulation of the last deglaciation using the Community Climate System Model, version 4 with realistic geometry and forcing conditions, including changes in insolation, greenhouse gases, continental ice sheets, and meltwater (Fig. 14 and *SI Appendix, Table S1*). Previous work has shown that the simulation successfully reproduces many observed features of the deglacial climate (4, 13, 20). In this way, the physical ocean environment of iPOP2-TRACE evolved in a similar way to TRACE21 (*SI Appendix, Fig. S3*). The $\delta^{18}\text{O}$ value of meltwater was prescribed as -31‰ in the Northern Hemisphere beginning 19 ka and -38‰ in the Southern Hemisphere beginning 14.35 ka. Details of the implementation and validation of the tracer module as well as the LGM spin up and the iPOP2-TRACE simulations are given in *SI Appendix* and the work by Zhang (21). A key feature of iPOP2-TRACE is its capability of quantifying the contribution of local water temperature to $\delta^{18}\text{O}_c$ (22), thus providing a dynamic framework for understanding the mechanisms responsible for the evolution of $\delta^{18}\text{O}_c$ during the last deglaciation.

Model Ocean Evolution and Isotopic Model-Data Comparison

In our model, strong AABW forms during the LGM caused by brine rejection associated with sea-ice expansion around Antarctica. The strong AABW formation along with a vigorous counterclockwise abyssal overturning cause the boundary between NADW and AABW to be shallower during the LGM (2.7 km) compared with today (3.3 km), with AABW filling most of the deep Atlantic (Fig. 2), consistent with paleonutrient tracers (23).

estimated uncertainty based on average deviation of adjacent measurements, and dashed lines represent three-point smoothing (6). Global mean $\delta^{18}\text{O}_{\text{w}}$ anomaly (gray) is converted from ice-volume equivalent sea level (45) by $1.05\text{‰}/145\text{ m}$. (G) Same as *F* but for deep water temperature anomalies based on Mg/Ca measurements (6, 32). All dashed lines indicate proxies, and solid lines indicate model results. B-A, Bølling-Allerød; PDB, Pee Dee Belemnite standard; SMOW, standard mean ocean water; YD, Younger Dryas.

During HS1, freshwater forcing nearly shuts down NADW transport (from 15 to 2.5 Sv; $\text{Sv} \equiv 10^6 \text{ m}^3 \text{ s}^{-1}$) (Fig. 1B). In contrast, AABW transport only decreases by 20% (Fig. 1C) because of surface warming and reduced brine rejection associated with significant sea-ice retreat in the SO (SI Appendix, Fig. S4), similar to other model simulations, which show little AABW response to a collapsed AMOC (24). The relative changes of water-mass volumes lead to further deep ocean occupation by AABW and a shoaling of the NADW–AABW boundary by $\sim 700 \text{ m}$ (Fig. 2C). The decrease in ventilation of the intermediate and deep NA by northern and southern sources results in it becoming largely isolated, with only slow renewal by AABW through the abyssal overturning. These simulated changes in NA ocean circulation are consistent with (i) various proxies that identify a reduced AMOC intensity (3, 25, 26) (Fig. 1B), (ii) the increased radiocarbon benthic–planktonic age offset at Iberian Margin (27) as a proxy for older apparent ventilation ages (Fig. 1D; radiocarbon simulation is given in SI Appendix), and (iii) benthic $\delta^{13}\text{C}$ proxies showing accumulation of respired carbon in the intermediate and deep NA (24). We suggest that ventilation of the deep SO increased during HS1 (5) because of greater air–sea interactions and release of low- ^{14}C CO_2 associated with sea-ice retreat (28, 29).

The simulated ocean circulation successfully reproduces the basin-wide pattern of the observed $\delta^{18}\text{O}_c$ changes across the intermediate and deep Atlantic between late HS1 and the LGM as constrained by 31 high-resolution, independently dated benthic $\delta^{18}\text{O}_c$ records [Fig. 3 and SI Appendix, Fig. S5 (with correlation $r = 0.82$)]. In particular, the model and data are characterized by the greatest changes in the upper NA and little change in the deep SO. The modeled $\delta^{18}\text{O}_c$ also captures several other observed $\delta^{18}\text{O}_c$ changes, such as in the middepth NA (8) and near the Brazil Margin (30) (SI Appendix), although it tends to overestimate the amplitude of $\delta^{18}\text{O}_c$ changes at intermediate depths (SI Appendix, Figs. S5 and S8), the causes and impact of which we discuss later.

To examine the regional phasing of the deep $\delta^{18}\text{O}_c$ response, we compared our simulation results with two well-dated, high-resolution benthic $\delta^{18}\text{O}_c$ records: one from the Iberian Margin in the NA (MD99-2334K; 37.8°N ; 3,146 m) (6, 31) and the other in the Atlantic sector of the SO (MD07-3076Q; 44.2°S ; 3,770 m) (5, 8). These cores also have bottom-water temperature reconstructions (6, 32), which, although having lower resolution and higher analytical uncertainty than the $\delta^{18}\text{O}_c$ data, allow for a general comparison. In both the model and the records (Fig. 1E), $\delta^{18}\text{O}_c$ shows a gradual postglacial increase from 22 to 19 ka, which is likely caused by the increase of $\delta^{18}\text{O}_w$ (Fig. 1F), since the water temperature remains unchanged during this period (Fig. 1G). The ocean reached its overall maximum $\delta^{18}\text{O}_w$ enrichment when ice sheets reached their maximum extent at $\sim 22 \text{ ka}$. The enrichment was not simultaneous throughout the global ocean, however, but

peaked sequentially from the surface to deep and across different ocean basins well after 22 ka (8, 33) (SI Appendix, Fig. S9) because of the long overturning timescale of the ocean from $\sim 1,500 \text{ y}$ in the Atlantic to more than 3,000 y in the Pacific.

From 19 to 16 ka, the modeled $\delta^{18}\text{O}_c$ captures the observed earlier and greater $\delta^{18}\text{O}_c$ decrease in the NA ($\sim 0.6\text{‰}$) than in the SO ($\sim 0.2\text{‰}$). The cause of this earlier $\delta^{18}\text{O}_c$ decrease at deep NA core sites during HS1 is widely debated. One “southern-source” hypothesis suggests that reduced formation of NADW during HS1 enhanced the formation and northward expansion of southern-sourced low- $\delta^{18}\text{O}$, low- $\delta^{13}\text{C}$ AABW (6, 7). An alternative “northern-source” hypothesis argues that, during HS1, the NA was influenced by overflows of brine-generated deep water formed by sea-ice expansion in the Nordic Seas, with the low $\delta^{18}\text{O}$ signal reflecting meltwater transferred to depth during brine formation (8–10) and the low $\delta^{13}\text{C}$ values reflecting suppressed air–sea gas exchange (8). Temperature may also have played a role in affecting the deglacial $\delta^{18}\text{O}_c$ signal, and increasing evidence of middepth warming in the NA during HS1 (20, 34, 35) implies that this warming should be taken into account to explain the middepth $\delta^{18}\text{O}_c$ decrease. In the deep Atlantic, however, a lack of high-resolution temperature reconstructions leads to large uncertainties in the sign and magnitude of temperature change in each hemisphere (7, 36) and in turn, its contribution to deep $\delta^{18}\text{O}_c$.

In this context, our model results indicate that the observed lead of the deglacial $\delta^{18}\text{O}_c$ decrease in the deep NA over the SO is caused by asynchronous warming of deep water rather than a change in the relative volume contributions of NADW and AABW, or their $\delta^{18}\text{O}_w$ values. During HS1, the simulated $\delta^{18}\text{O}_w$ component shows nearly coherent decreases at both core sites (Fig. 1F). These depletions at depth are caused primarily by the transfer of ^{18}O -depleted surface meltwater, with a change of surface precipitation and evaporation playing a minor role (SI Appendix, Fig. S10). Although the decrease of NA $\delta^{18}\text{O}_w$ is slightly greater, since the site is geographically closer to the meltwater source, the difference is nearly indistinguishable and cannot explain the much larger differences seen in the records. In contrast, the temperature component exhibits strong asynchrony, with the deep ocean below 3,000 m warming by $\sim 1.4^\circ \text{C}$ in the north but experiencing little change in the south, roughly consistent with Mg/Ca temperature reconstructions (6, 32) (Fig. 1G). The warming in the north causes $\delta^{18}\text{O}_c$ to decrease by $\sim 0.35\text{‰}$, thus explaining most of the 0.4‰ difference between the two records.

The relative contributions of $\delta^{18}\text{O}_w$ and temperature can be seen more clearly in the basin-wide responses. In response to the input of ^{18}O -depleted freshwater during HS1, $\delta^{18}\text{O}_w$ decreases over the entire basin relative to its LGM values (Fig. 4E), similar to the salinity response. A considerable portion of the ^{18}O -depleted freshwater is trapped in the upper NA and within the Labrador Sea and the Nordic Seas (Fig. 4C). An anomalous tongue of modest size

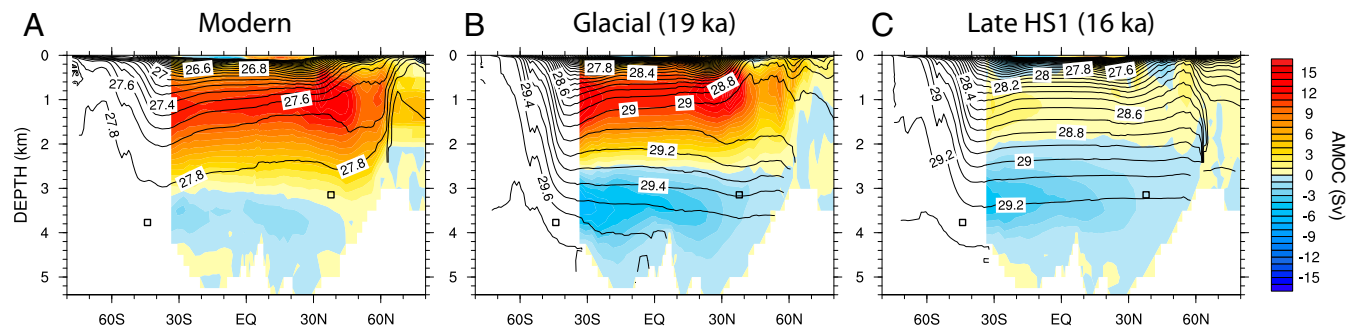


Fig. 2. Atlantic total meridional overturning circulation at modern (A), glacial at 19 ka (B), and late HS1 at 16 ka (C). Total circulation, also known as residual circulation, is the sum of the Eulerian mean circulation and the circulation caused by mesoscale eddies (submesoscale eddies are ignored, since they are small and concentrated at surface layers) and is directly related to tracer transport. The Atlantic zonal mean potential densities (σ_θ) of each period are overlaid in black contours, with intervals of 0.1 kg m^{-3} . Squares indicate the two cores sites of Fig. 1E.

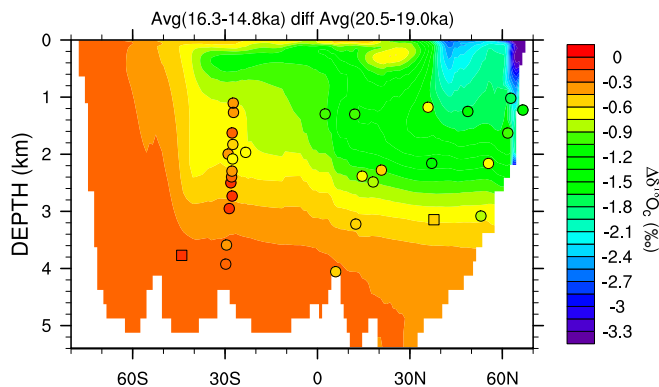


Fig. 3. Deglacial benthic $\delta^{18}\text{O}_a$ changes in the Atlantic. Contours are zonally averaged Atlantic $\delta^{18}\text{O}_a$ changes between late HS1 (16.3–14.8 ka mean) and glacial (20.5–19.0 ka mean) periods in the model. Circles and squares are reconstructed benthic $\delta^{18}\text{O}_a$ changes at 31 independently dated core sites (SI Appendix, Table S2) between these two periods. Squares indicate the two core sites of Fig. 1E.

($\sim 0.1\text{‰}$) extends downward and southward along the lower limb of the diminishing glacial AMOC during the transition to HS1 and further disperses into the whole ocean through residual circulation and mixing (Fig. 4E). This $\delta^{18}\text{O}_w$ response in the Atlantic basin is similar to what has previously been simulated in a model of intermediate complexity (12). In contrast, the temperature field shows a bipolar seesaw response at the surface and basin-wide warming in the subsurface (Fig. 4F), consistent with observations (20, 34, 35). Notably, the warming occurs all of the way to the abyss in the NA but not in the SO, generating a deep meridional temperature gradient that accounts for the $\delta^{18}\text{O}_a$ gradient across the deep Atlantic.

Mechanisms of Tracer Evolution During HS1

The Impact of Circulation on $\delta^{18}\text{O}_w$ Distribution. We conducted two sensitivity experiments to separate the circulation effect from the boundary effect on $\delta^{18}\text{O}_w$ distribution. One experiment (iPOP2-19ka) simulated $\delta^{18}\text{O}_w$ with transient surface forcing from 19 to 16 ka but with the circulation held at the 19-ka level. This was achieved by looping the boundary conditions of 20–19 ka of TRACE21 but applying the transient $\delta^{18}\text{O}_w$ surface fluxes taken from iPOP2-TRACE. The other experiment (iPOP2-0ka) was similar to iPOP2-19ka but with a modern circulation pattern forced by interannually varying atmospheric dataset of the Coordinated Ocean-Ice Reference Experiments phase II (37).

When the circulation is held at its 19-ka level, the low- $\delta^{18}\text{O}$ signal is no longer able to accumulate in the upper NA during HS1 as in iPOP2-TRACE (Fig. 4E) but is well-distributed in the whole Atlantic (Fig. 4G) and extends to the Pacific and Indian oceans. This suggests that the strong reduction in NADW formation and associated overflows is the direct cause of the trapped ^{18}O -depleted water in iPOP2-TRACE. We also note that the tongue of southward expansion of the ^{18}O -depleted water is confined to above 3,000 m in iPOP2-19ka (Fig. 4G), even with a strong and fully functional AMOC. This is because NADW is confined above the thick abyssal layer of AABW (Fig. 2B). In contrast, the expansion of the low- $\delta^{18}\text{O}$ tongue in iPOP2-0ka reaches deeper in the NA with more tilted contours (Fig. 4H), consistent with the modern AMOC pattern (Fig. 24).

Physical Processes at the Two Core Sites. We conducted a tracer budget analysis to identify the specific physical processes as responsible for the different $\delta^{18}\text{O}_w$ and temperature responses during HS1 (SI Appendix). During the LGM, $\delta^{18}\text{O}_w$ is increasingly depleted with depth in the northern NA, while during HS1, this vertical gradient reverses because of the input of highly ^{18}O -depleted freshwater at the surface (Fig. 5A). The $\delta^{18}\text{O}_w$

budget at 3,100 m shows a regime shift during HS1 to a dominant balance between two vertical processes, namely vertical mixing and vertical advection, and an over 90% decrease of the horizontal advective fluxes (Fig. 5B). The surface low- $\delta^{18}\text{O}$ signal weakens with depth, because vertical mixing takes a long time to transfer the signal from the surface down to 3,100 m in the absence of deep convection. The deep NA, therefore, experiences little $\delta^{18}\text{O}_w$ change, although it is geographically close to the freshwater input. In contrast, the $\delta^{18}\text{O}_w$ in the SO has a mild, vertically uniform transition (Fig. 5C), and the regime shift of the $\delta^{18}\text{O}_w$ budget found in the northern NA does not occur in the deep SO (Fig. 5D).

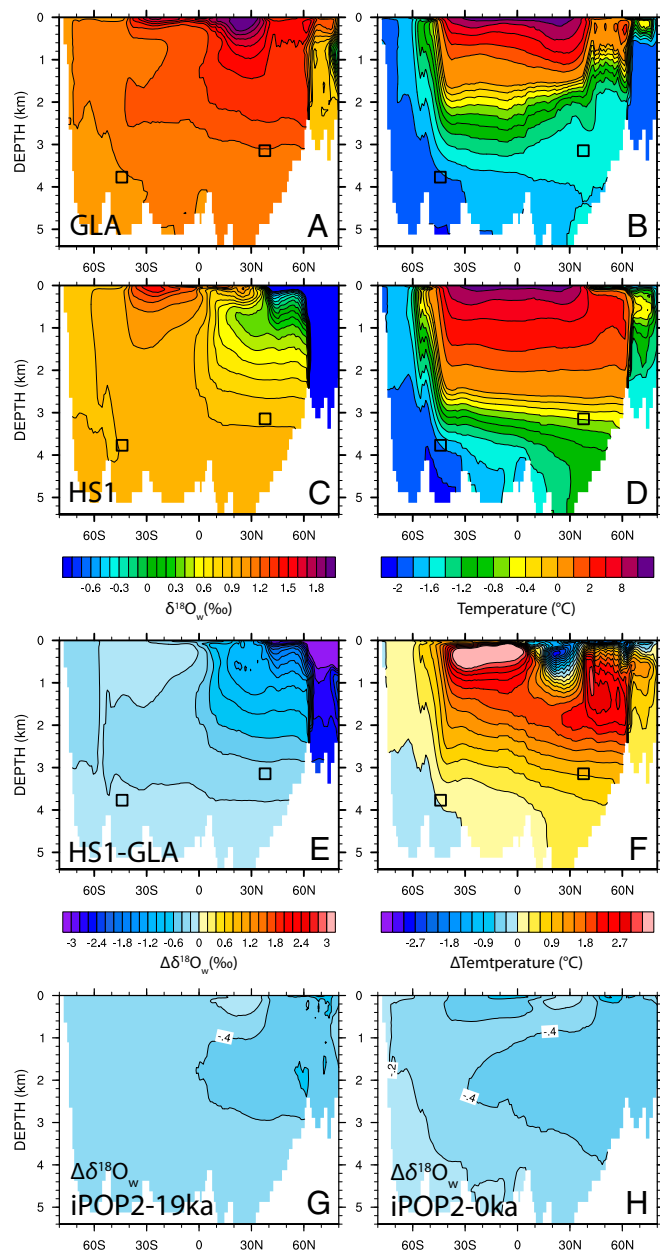


Fig. 4. (A–F) Atlantic zonally averaged $\delta^{18}\text{O}_w$ (A, C, and E) and potential temperature (B, D, and F). Panels are variables at 19 ka (A and B), 16 ka (C and D), and their differences (E and F). Squares indicate the two core sites of Fig. 1E. Note that the color bar for B and D is nonlinear. The deep NA core site experiences reversed $\delta^{18}\text{O}_w$ vertical gradient and enlarged temperature vertical gradient from 19 to 16 ka. (G and H) The $\delta^{18}\text{O}_w$ differences between 16 and 19 ka of the two sensitivity experiments iPOP2-19ka and iPOP2-0ka (sharing the same color bar with E).

and enhanced downward heat flux via vertical mixing that transfers heat from intermediate depths to the deep ocean.

Our proposed warming mechanism has two major differences from previous studies. Some previous studies (e.g., “deep decoupling oscillation”) suggested that the NA middepth warming originated from diffusion of tropical ocean heat across the main thermocline and transported northward (20, 35, 40–42). If the heat were from the tropics, the NA isotherms would deepen gradually from the depth of the main thermocline (~300–500 m) to lower layers and would probably lag the freshwater event by decades or even longer (40). However, our model suggests that the middepth warming occurs first at 2,000 m and immediately with the freshwater forcing onset. We thus argue that the northern NA middepth warming is caused largely by the shoaling of winter season deep convection depth. Additional supporting evidence is that another rapid middepth warming occurs at 17.4–17.2 ka (Fig. 5E), when isotherms between 400 and 1,300 m experience a sudden deepening, corresponding to a second rapid shoaling of the deep convection depth from 1,300 to 400 m (SI Appendix, Fig. S12D) in response to the increased rate of freshwater forcing (Fig. 1A). This physical process may be used to explain the large and abrupt warming at 2,000-m depth during HS1 observed in deep sea corals in the western NA as well as the contemporaneous shift to more ^{14}C -depleted waters (34) (SI Appendix, Fig. S13), although the observed abrupt warming and aging occurred later than in the model.

The second notable difference between our mechanism and the deep decoupling oscillation is that the latter suggests that the reduced AMOC causes a diffusive warming of the deep ocean by a reduction in the upwelling of cold water (40, 43). However, our heat-budget analysis shows an enhanced cooling effect from the upwelling (Fig. 5E). The upwelling velocity (w) indeed decreases, but the increase of the vertical temperature gradient ($\partial T/\partial z$) is so large that it overwhelms the velocity effect and causes the vertical advective cooling ($w\partial T/\partial z$) to increase (SI Appendix, Fig. S14). Both the vertical mixing and vertical advection are actually enhanced by this increased $\partial T/\partial z$, with the former enhanced more. We thus conclude that it is the enhanced downward heat transport via vertical mixing rather than the reduced upwelling of cold water that effectively heats the deep NA.

ACKNOWLEDGMENTS. We thank B. Otto-Bliesner for her support throughout the work; J. Gottschalk, S. Gu, J. Zhu, and A. Hu for helpful discussions; G. Danabasoglu, D. Bailey, and S. Bates for modeling technical assistance; and J. Roberts, D. Lund, L. Skinner, and S. Weldeab for providing data. This work is supported by US National Science Foundation (NSF) Projects 1401778, 1401802, 1600080, and 1566432; US Department of Energy Project DE-SC0006744, the Regional and Global Climate Modeling program, and the Center for Nonlinear Studies sponsored by Laboratory Directed Research and Development; National Natural Science Foundation of China Grant 41630527; and the Wisconsin Alumni Research Foundation. Computing resources were provided by the Climate Simulation Laboratory at the National Center for Atmospheric Research's Computational and Information Systems Laboratory sponsored by the US NSF and other agencies.

- Broecker WS (1998) Paleocan circulation during the last deglaciation: A bipolar seesaw? *Paleoceanography* 13:119–121.
- Roberts NL, Piotrowski AM, McManus JF, Keigwin LD (2010) Synchronous deglacial overturning and water mass source changes. *Science* 327:75–78.
- McManus JF, Francois R, Gherard J-M, Keigwin LD, Brown-Leger S (2004) Collapse and rapid resumption of Atlantic meridional circulation linked to deglacial climate changes. *Nature* 428:834–837.
- Shakun JD, et al. (2012) Global warming preceded by increasing carbon dioxide concentrations during the last deglaciation. *Nature* 484:49–54.
- Skinner LC, Fallon S, Waelbroeck C, Michel E, Barker S (2010) Ventilation of the deep Southern Ocean and deglacial CO_2 rise. *Science* 328:1147–1151.
- Skinner LC, Shackleton NJ, Elderfield H (2003) Millennial-scale variability of deep-water temperature and $\delta^{18}\text{O}_{\text{dw}}$ indicating deep-water source variations in the Northeast Atlantic, 0–34 cal. ka BP. *Geochim Geophys Geosyst* 4:1098.
- Skinner LC, Shackleton NJ (2006) Deconstructing terminations I and II: Revisiting the glacioeustatic paradigm based on deep-water temperature estimates. *Quat Sci Rev* 25:3312–3321.
- Waelbroeck C, et al. (2011) The timing of deglacial circulation changes in the Atlantic. *Paleoceanography* 26:PA3213.
- Meland MY, Dokken TM, Jansen E, Høyevåg K (2008) Water mass properties and exchange between the Nordic seas and the northern North Atlantic during the period 23–6 ka: Benthic oxygen isotopic evidence. *Paleoceanography* 23:PA1210.
- Thornalley DJR, Elderfield H, McCave IN (2010) Intermediate and deep water paleoceanography of the northern North Atlantic over the past 21,000 years. *Paleoceanography* 25:PA1211.
- Lea DW (2014) Elemental and isotopic proxies of past ocean temperatures. *Treatise on Geochemistry*, eds Holland HD, Turekian KK (Elsevier, Amsterdam), 2nd Ed, pp 373–397.
- Ganopolski A, Roche DM (2009) On the nature of lead-lag relationships during glacial-interglacial climate transitions. *Quat Sci Rev* 28:3361–3378.
- Liu Z, et al. (2009) Transient simulation of last deglaciation with a new mechanism for Bolling-Allerød warming. *Science* 325:310–314.
- Smith RS, Gregory J (2012) The last glacial cycle: Transient simulations with an AOGCM. *Clim Dyn* 38:1545–1559.
- Friedrich T, Timmermann A (2012) Millennial-scale glacial meltwater pulses and their effect on the spatiotemporal benthic $\delta^{18}\text{O}$ variability. *Paleoceanography* 27:PA3215.
- Roche DM, Paillard D, Caley T, Waelbroeck C (2014) LGM hosing approach to Heinrich event 1: Results and perspectives from data-model integration using water isotopes. *Quat Sci Rev* 106:247–261.
- Bagniewski W, Meissner KJ, Menviel L, Brennan CE (2015) Quantification of factors impacting seawater and calcite $\delta^{18}\text{O}$ during Heinrich Stadials 1 and 4. *Paleoceanography* 30:895–911.
- Liu Z, et al. (2014) Chinese cave records and the East Asia summer monsoon. *Quat Sci Rev* 83:115–128.
- Schrag DP, et al. (2002) The oxygen isotopic composition of seawater during the last glacial maximum. *Quat Sci Rev* 21:331–342.
- Marcott SA, et al. (2011) Ice-shelf collapse from subsurface warming as a trigger for Heinrich events. *Proc Natl Acad Sci USA* 108:13415–13419.
- Zhang J (2016) Understanding the deglacial evolution of deep Atlantic water masses in an isotope-enabled ocean model. PhD dissertation (University of Wisconsin–Madison, Madison, WI).
- Marchitto TM, et al. (2014) Improved oxygen isotope temperature calibrations for cosmopolitan benthic foraminifera. *Geochim Cosmochim Acta* 130:1–11.
- Curry WB, Oppo DW (2005) Glacial water mass geometry and the distribution of $\delta^{13}\text{C}$ of SCO_2 in the western Atlantic Ocean. *Paleoceanography* 20:PA1017.
- Schmittner A, Lund DC (2015) Early deglacial Atlantic overturning decline and its role in atmospheric CO_2 rise inferred from carbon isotopes ($\delta^{13}\text{C}$). *Clim Past* 11:135–152.
- Clark PU, et al. (2012) Global climate evolution during the last deglaciation. *Proc Natl Acad Sci USA* 109:E1134–E1142.
- Buizert C, et al. (2014) Greenland temperature response to climate forcing during the last deglaciation. *Science* 345:1177–1180.
- Skinner LC, Waelbroeck C, Scrivner AE, Fallon SJ (2014) Radiocarbon evidence for alternating northern and southern sources of ventilation of the deep Atlantic carbon pool during the last deglaciation. *Proc Natl Acad Sci USA* 111:5480–5484.
- Keeling RF, Stephens BB (2001) Antarctic sea ice and the control of Pleistocene climate instability. *Paleoceanography* 16:112–131.
- Sigman DM, Hain MP, Haug GH (2010) The polar ocean and glacial cycles in atmospheric CO_2 concentration. *Nature* 466:47–55.
- Lund DC, Tessin AC, Hoffman JL, Schmittner A (2015) Southwest Atlantic water mass evolution during the last deglaciation. *Paleoceanography* 30:477–494.
- Skinner LC, Shackleton NJ (2004) Rapid transient changes in northeast Atlantic deep water ventilation age across termination I. *Paleoceanography* 19:PA2005.
- Roberts J, et al. (2016) Evolution of South Atlantic density and chemical stratification across the last deglaciation. *Proc Natl Acad Sci USA* 113:514–519.
- Stern JV, Lisiecki LE (2014) Termination 1 timing in radiocarbon-dated regional benthic $\delta^{18}\text{O}$ stacks. *Paleoceanography* 29:1127–1142.
- Thiagarajan N, Subhas AV, Southon JR, Eiler JM, Adkins JF (2014) Abrupt pre-Bolling-Allerød warming and circulation changes in the deep ocean. *Nature* 511:75–78.
- Weldeab S, Friedrich T, Timmermann A, Schneider RR (2016) Strong middepth warming and weak radiocarbon imprints in the equatorial Atlantic during Heinrich 1 and Younger Dryas. *Paleoceanography* 31:1070–1082.
- Oppo DW, Curry WB, McManus JF (2015) What do benthic $\delta^{13}\text{C}$ and $\delta^{18}\text{O}$ data tell us about Atlantic circulation during Heinrich Stadial 1? *Paleoceanography* 30:353–368.
- Griffies SM, et al. (2012) Datasets and protocol for the CLIVAR WGOMD Coordinated Ocean-sea ice Reference Experiments (COREs). Available at data1.gfdl.noaa.gov/~nnz/mom4/COREv2/doc/CORE_notes.23oct2012.pdf. Accessed October 23, 2012.
- Henning CC, Vallis GK (2005) The effects of mesoscale eddies on the stratification and transport of an ocean with a circumpolar channel. *J Phys Oceanogr* 35:880–896.
- Condon A, Winsor P (2012) Meltwater routing and the Younger Dryas. *Proc Natl Acad Sci USA* 109:19928–19933.
- Winton M, Sarachik ES (1993) Thermohaline oscillations induced by strong steady salinity forcing of ocean general circulation models. *J Phys Oceanogr* 23:1389–1410.
- Olsen SM, Shaffer G, Bjerrum CJ (2005) Ocean oxygen isotope constraints on mechanisms for millennial-scale climate variability. *Paleoceanography* 20:PA1014.
- Mignot J, Ganopolski A, Levermann A (2007) Atlantic subsurface temperatures: Response to a shutdown of the overturning circulation and consequences for its recovery. *J Clim* 20:4884–4898.
- Palter JB, et al. (2014) The deep ocean buoyancy budget and its temporal variability. *J Clim* 27:551–573.
- Jahn A, et al. (2015) Carbon isotopes in the ocean model of the Community Earth System Model (CESM1). *Geosci Model Dev* 8:2419–2434.
- Lambeck K, Roubey H, Purcell A, Sun Y, Sambridge M (2014) Sea level and global ice volumes from the last glacial maximum to the Holocene. *Proc Natl Acad Sci USA* 111:15296–15303.